Available online at www.sciencedirect.com
ScienceDirect
Journal of Solid State Chemistry 180 (2007) 2034–2043
JOURNAL OF SOLID STATE CHEMISTRY
www.elsevier.com/locate/jssc

An in situ time-of-flight neutron powder diffraction study of the humidity-induced phase transition in sodium monothiophosphate

Nathan J. Takas, Jennifer A. Aitken*

Department of Chemistry and Biochemistry, Duquesne University, Pittsburgh, PA 15282, USA

Received 13 March 2007; received in revised form 7 May 2007; accepted 14 May 2007
Available online 18 May 2007

Abstract

Anhydrous β-Na_3PO_3S, obtained by rapid cooling, has been observed to convert to the more thermodynamically stable, anhydrous α-Na_3PO_3S upon exposure to a humid atmosphere. Though water plays a critical role in this polymorphic transformation, it is absent in both the initial and final materials. In situ time-of-flight neutron powder diffraction was used to track the progress of this transition as a function of time. Diffraction data were acquired using the Intense Pulsed Neutron Source (IPNS) at Argonne National Laboratory. An empirical whole pattern fitting method was used to determine the polymorphic phase composition over time. The resulting data were evaluated using several solid-state kinetic models. The kinetics of this transition has been determined to be best described by either one- or two-dimensional diffusion. The significance of these models with respect to the physical phenomenon is discussed.

Keywords: Humidity; Phase change; Phase transition; Neutron diffraction; Sulfide; Oxythiophosphate; Diffusion; Powder diffraction; Whole pattern fitting

1. Introduction

The earliest discovered oxythiophosphate material was sodium monothiophosphate dodecahydrate, $Na_3PO_3S \cdot 12H_2O$, having been synthesized over 160 years ago [1,2]. The anhydrous salt of sodium monothiophosphate was first prepared in 1940 by Zintl and Bertram [3]. The structure of this phase was recently solved by Jansen et al. through the use of X-ray and neutron powder diffraction methods [4]. Despite this long history, there are still many interesting properties to be discovered with respect to this material [5].

Our work is currently focused on the use of sodium monothiophosphate as a starting material for the preparation of new, more complex metal oxythiophosphate materials. However, before venturing into these more diverse systems, it became imperative that we study sodium monothiophosphate, the precursor salt. In the process, an unusual transition between anhydrous crystalline phases, facilitated by atmospheric water, was observed [5].

Spontaneous isothermal phase transitions must involve conversion to a more thermodynamically stable phase to supply a thermodynamic driving force for the conversion. The humidity-induced phase transition reported here is no exception, as it is observed to occur from a sample of β-Na_3PO_3S [5,6], obtained by fast cooling from high temperatures, to α-Na_3PO_3S, the room temperature stable phase.

Phase transitions induced by exposure to a humid atmosphere are not unusual [7–14], however, these transitions typically involve conversion between an anhydrous and a hydrated phase [7,11–14]. Conversions between anhydrous phases have been observed among small molecule organic solids. More research on these solids has been carried out in support of the pharmaceutical industry due to the importance of the relationships between polymorphism, physical stability and bioavailability [7,15–17]. However, these transitions are most often from an amorphous to a crystalline state [9,18,19]. Among inorganic materials, observations of anhydrous crystalline to anhydrous crystalline phase transitions catalyzed by atmospheric water are rare. In fact, the only such report known to these authors is that of humidity-induced

*Corresponding author. Fax: +1 412 396 5683.
E-mail address: aitkenj@duq.edu (J.A. Aitken).

0022-4596/$ - see front matter © 2007 Elsevier Inc. All rights reserved.
doi:10.1016/j.jssc.2007.05.011

polymorphic transitions between the high- and low-temperature phases of lithium, sodium and potassium formate [20]. In this report, it was observed that the high-temperature phases of these formates, trapped by rapid cooling, transformed to the low-temperature phases relatively quickly upon exposure to a humid atmosphere, despite the fact that the quenched high-temperature phases were found to persist under vacuum. Unfortunately, no detailed study of the transformation, measurements of the process, or discussion of a potential mechanism was put forth.

Knowing that these transitions are rare in the inorganic literature, in situ neutron diffraction experiments were carried out at the Intense Pulsed Neutron Source (IPNS) at Argonne National Lab under controlled humidity conditions to better characterize this phenomenon. This report will describe the treatment of the acquired neutron diffraction data by an empirical whole pattern fitting method, the model fitting process to determine appropriate solid-state kinetic models, and an interpretation of the physical meaning of these models in regard to this particular solid-state phenomenon.

2. Experimental

2.1. Synthesis

2.1.1. Synthesis of α-Na_3PO_3S

α-Na_3PO_3S was prepared by hydrolysis of $PSCl_3$ in an aqueous solution of NaOH, followed by dehydration via suspension in anhydrous methanol, as described elsewhere [5,21]. The product obtained by this method is a fine white powder and further grinding is not necessary prior to transferring of this material to the vanadium canister for neutron diffraction measurements.

2.1.2. Synthesis of β-Na_3PO_3S

A sample of β-Na_3PO_3S was obtained by heating approximately 0.4 g α-Na_3PO_3S in a fused-silica tube, sealed under vacuum ($\sim10^{-3}$ mbar), to 600 °C at a rate of 10 °C/min in a programmable furnace and allowing it to equilibrate for 30 min. The sample was then rapidly cooled by immersion of the sealed tube in an ice water bath to obtain a quenched sample of β-Na_3PO_3S having a sintered morphology. This process was repeated multiple times to obtain a satisfactory amount of material for neutron powder diffraction experiments. Several grams of the quenched sample of β-Na_3PO_3S were ground using a mortar and pestle in a helium filled glovebag before being transferred to the vanadium sample canister for neutron diffraction measurements (see Section 2.2.3).

2.2. Physical measurements

2.2.1. Differential thermal analysis

Differential thermal analysis (DTA) was performed using a Shimadzu DTA-50, which was calibrated using a three-point calibration curve based on the melting points of indium, zinc and gold metals. The differential signal was balanced prior to the beginning of each experiment. Data were recorded using the Shimadzu TA60-WS collection program. Experiments were performed at a rate of 10 °C/min. Samples were contained in carbon-coated fused-silica ampoules sealed under vacuum ($\sim10^{-3}$ mbar). All DTA samples were referenced against an alumina sample, contained similarly and of comparable mass. Multiple heating and cooling cycles were performed in the DTA experiments to differentiate between reversible and irreversible thermal events.

2.2.2. Powder X-ray diffraction

Powder X-ray diffraction (PXRD) patterns were obtained on a Rigaku D/max-B, powder X-ray diffractometer, model number D2013, using copper K_α radiation and operating at 35 kV and 22.5 mA. Samples were prepared by adhering the sample to double-sided tape over a glass specimen slide. All diffraction patterns were collected from 10° to 70° in 2θ using a step size of 0.024° at a scan rate of 2°/min.

2.2.3. General neutron diffraction

Neutron diffraction experiments on the polymorphs of Na_3PO_3S were conducted using the General Purpose Powder Diffractometer (GPPD) at the IPNS located in Argonne National Laboratory. All samples were prepared in a helium-filled glovebag and loaded into vanadium canisters for data collection.

2.2.3.1. High temperature neutron diffraction. A sample of several grams of α-Na_3PO_3S was used, as prepared, and loaded into a 7/16 in vanadium canister under a helium atmosphere. The canister was covered with parafilm to minimize exposure to air during transfer to the instrument. The sample was placed in the Howe furnace [22], a vanadium foil resistive-element furnace, and evacuated. Once a desirable vacuum had been achieved ($<10^{-5}$ mbar), a neutron powder diffraction pattern of α-Na_3PO_3S was obtained at room-temperature over the course of 259,334 pulses. This neutron diffractogram will hereafter be referred to as the "α-phase reference pattern".

The sample was next heated from room temperature to 600 °C at a rate of 8 °C/min. The sample was allowed to equilibrate at this temperature until diffraction of the α-phase was no longer observed, and a diffraction pattern corresponding to the γ-phase was readily apparent. A neutron diffraction pattern of the γ-phase was obtained by summing 20 diffractograms, which were each acquired for ~54,000 pulses or ~30 min each, giving a total of 1,080,160 pulses. The sample was next cooled to 505 °C at a rate of 8 °C/min, and equilibrated at this temperature until diffraction of the γ-phase was no longer observed, and diffraction of the β-phase became readily apparent. A neutron diffraction pattern of the β-phase was obtained by summing 15 diffractograms, which were each acquired for

~54,000 pulses or ~30 min each, giving a total of 810,108 pulses. The program ISAW [23] was used to sum the various diffractograms acquired throughout the course of each experiment.

2.2.2.2. Controlled humidity neutron diffraction. The experimental setup to measure the humidity-catalyzed phase transition between β- and α-Na_3PO_3S was developed specifically for this experiment [24] (see Fig. 1). Two dry nitrogen gas cylinders were each manipulated through the use of computer controlled mass flow controllers. One of these dry N_2 lines was bubbled through one linear centimeter of D_2O to obtain a humidified gas flow, while the second N_2 line remained dry. The two gases were then combined, and their relative flow rates adjusted to calibrate a variable-humidity gas flow.

The sample of β-Na_3PO_3S, obtained by quenching, was contained in a vanadium tube with glass wool plugs at both the top and bottom. The sample was first placed in the stream with only dry gas flowing to acquire a single reference pattern of the β-phase prior to any transformation. This diffractogram will hereafter be known as the "β-phase reference pattern", which was collected for ~54,000 pulses on the same sample that was later induced to convert to the α-phase by exposure to a humid gas flow. Once the β-phase reference pattern was collected, the humid gas flow was initiated with predetermined flow rates to provide a relative humidity (RH) of 35%. 51 Neutron diffractograms of the transition were collected for ~54,000 pulses or ~30 min each (see Fig. 2). One single diffractogram during the transition was collected for a larger number of pulses, 79,894. All data used for whole pattern fitting were taken from detector bank 5 centered at 53°. All controlled humidity neutron diffraction data reported herein were collected at an ambient temperature of 29 °C.

Initial observations of the outgas humidity, were far lower than the anticipated value of 35% RH. However, the outgas humidity was observed to change over time, eventually climbing up to 45% RH (see Fig. 3). At the end of data collection, the sample was removed from the gas stream and the outgas humidity was directly measured to be 33% RH, a value which is very near the set humidity of 35% RH and within the acceptable limits of the uncertainty of the hygrometer probe.

3. Results

3.1. Data treatment

The phase composition of the sample through time was determined by an empirical whole pattern fitting method. The whole pattern fitting method was used by assuming that the absence of a third phase during the transition meant that the transition represents a strictly two-phase system, an assumption that the refinements seem to support. This model seems applicable since, at no time during the transformation, was any diffraction pattern observed other than those corresponding to the α- and β-phases of sodium monothiophosphate. All of the measured diffraction patterns were thus assumed to be

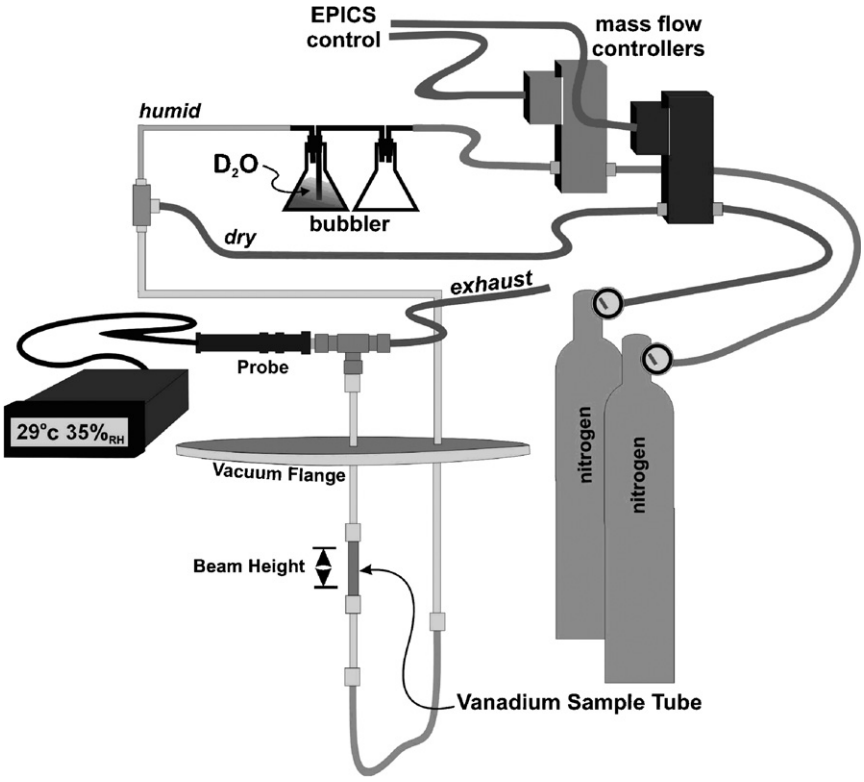

Fig. 1. Diagram of the controlled humidity apparatus used for in situ neutron powder diffraction experiments.

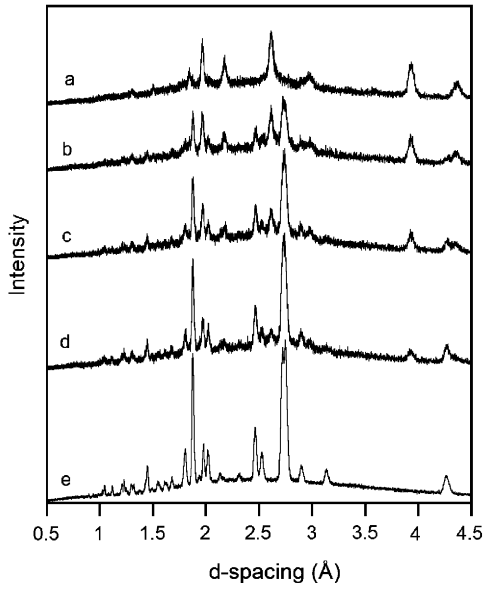

Fig. 2. Neutron powder diffractograms of the sample throughout the transition from pure β-Na_3PO_3S (a) to α-Na_3PO_3S (e). The midpoints, b, c and d represent the sample at approximately 30%, 50% and 70% conversion to the α-phase, respectively.

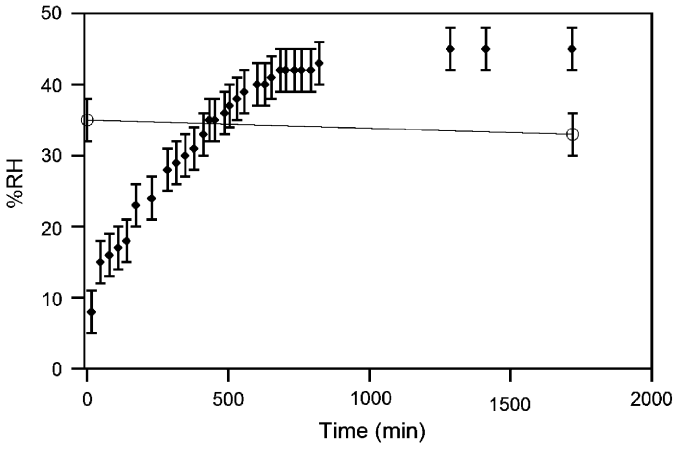

Fig. 3. Outgas humidity measured as a function of time. The open circle data points represent the humidity of the outgas measured without the sample in the gas stream both before and after experimentation.

readily modeled as some mole fraction of the β-phase (X), and the complimentary mole fraction of the α-phase ($1-X$). The use of two-phase Rietveld refinement would have been preferred over an empirical whole pattern fitting method; however, Rietveld refinement requires knowledge of all structures involved, and the structure of the β-phase has, so far, eluded us and others [6].

3.1.1. Model development

The assumption of the two-phase system can be generally modeled in the manner described by Eq. (1), assuming a constant flux of diffracted particles, either photons or neutrons. In this equation, $I_m(d)$ is the intensity predicted by the model as a function of d-spacing, $I_\beta(d)$ and $I_\alpha(d)$ are the intensities of the β- and α-phase reference patterns respectively as a function of d-spacing, and X is the average mole fraction of the β-phase present in the sample during the time interval being measured

$$I_m(d) = XI_\beta(d) + (1 - X)I_\alpha(d). \quad (1)$$

The diffraction data in question, however, were acquired using a pulsed neutron source, which is susceptible to changes in total neutron flux over time. As such, several scaling factors were introduced to accommodate changes in total flux. These scaling factors force the adaptation of Eq. (1) to the form in Eq. (2). In this equation, F_{ref} is a scaling factor which allows for differences in measured flux between reference patterns and F_{tot} is a scaling factor which scales the entire model to allow for variations between the reference patterns and the individual diffractograms measured during the transition

$$I_m(d) = F_{tot}\{[XI_\beta(d)] + F_{ref}[(1 - X)I_\alpha(d)]\}. \quad (2)$$

The best-fit model was determined by the minimization of the crystallographic R factor as defined as [25]

$$R = \frac{\int [I_{meas}(Q) - I_{calc}(Q)]^2 \, dQ}{\int [I_{meas}(Q)]^2 \, dQ}, \quad (3)$$

where Q [25] is defined as:

$$Q = \frac{4\pi * \sin(\theta)}{\lambda} = \frac{2\pi}{d}.$$

Diffraction data corresponding to the α-phase reference pattern, the β-phase reference pattern, and an experimental pattern, whose composition was to be determined, were copied into a single Excel spreadsheet [26]. Excel Solver, using a generalized reduced gradient method [27], was employed to determine the values of X, F_{ref}, and F_{tot}, which would provide the lowest value of the crystallographic R factor (see Fig. 4). A zero-point correction was also manually applied to the α-phase reference pattern to minimize the crystallographic R factor. A numerical columnar integration method was employed, since more sophisticated numerical integration methods assume the data to be a smooth, continuous function, which, in this case, it is not.

The refinement of the three variables proceeded as follows. The value of F_{ref} was determined only once, based on a sample measured at late experimental time, when dX/dt is minimal. The value of this refined parameter was determined for several other data points, but was not found to change significantly. Therefore, this parameter was not refined for other data points, but was applied as a fixed scaling factor. The values of X and F_{tot} were refined for each point in time independently.

β- to α-phase kinetics were modeled by plotting the mole percent converted (α-phase) versus the mean time of that pattern's data collection period (see Fig. 5). It should be noted that while this choice of time placement is not rigorously accurate, given the potential variations in neutron flux over time, it is an adequate approximation.

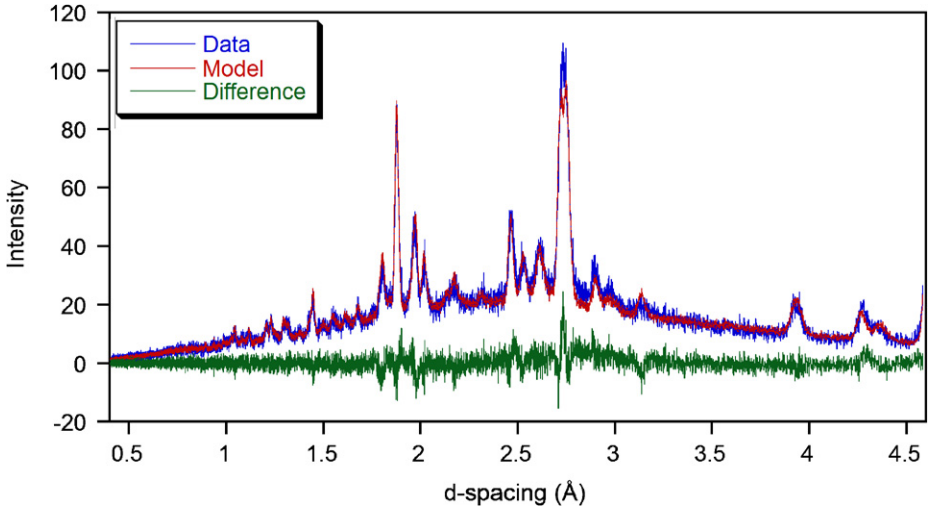

Fig. 4. One of the neutron diffractograms from the whole pattern fitting process. The displayed diffractogram corresponds to 1003 min exposure to deuterated humid atmosphere and 58.75% conversion to the α-phase. The crystallographic R factor of this model is 1.67%.

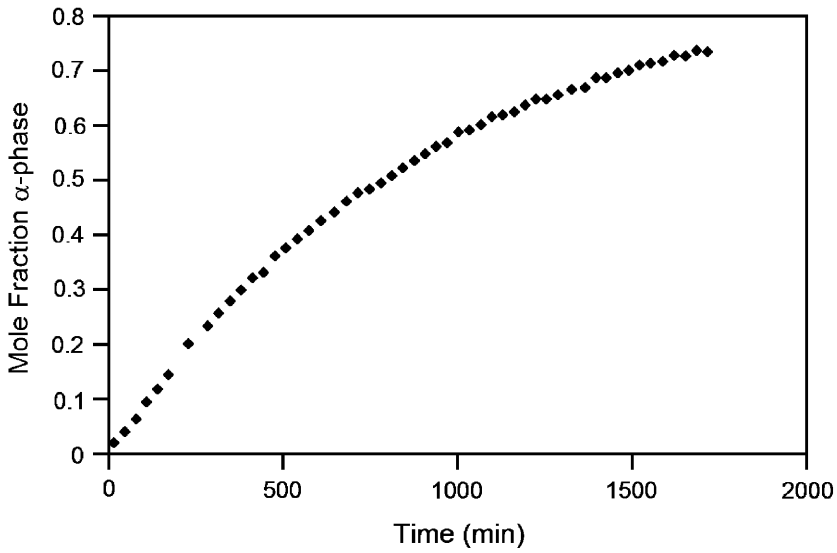

Fig. 5. Kinetic data describing the polymorphic phase transition through time.

Eleven solid-state kinetic models [7] were linearized and the kinetic data were applied to each.

It is strictly impossible to determine the mechanism by which a solid-state reaction proceeds simply by determining which model forms the best fit line when it is applied; however, it is possible to rule out a model due to clearly poor intercepts, slopes, or R^2 values. Several models were therefore discarded, due to a failure to accurately describe the transformation. The Prout-Tompkins, one-dimensional advance of phase boundary, and the four power laws [7] that were used, were discarded due to the unrealistic y-intercepts predicted and the generally poor fit of the data by analytical and graphical inspection (see Table 1). All models should theoretically intercept the y-axis very near to zero, except the one-dimensional advance of phase boundary model, which should intercept the y-axis very near to one.

The remaining five models were evaluated in the following manner. The idealized linear model was used to calculate a theoretical time for each of the measured percent compositions. The actual time of the measurement was then subtracted from this theoretical value to give a Δt between the model and the experimental data to obtain a graph of Δt vs. t. If a certain model was truly representative of the system, the graph of Δt vs. t should be found to vary linearly with time, if the slope and intercept of the theoretical line are inaccurate. However, in the case that the slope and intercept of the theoretical line are accurate, the Δt vs. t line should have a slope of 0 and no data point should vary from 0 by more than ± 15 min (see Fig. 6 (top)). The model/data time drift is allowed this window because most data were collected over a time period of ~30 min, and the data were plotted at the center point of this collection time frame. If the equation of the model

Table 1
Summary of the linearization of all kinetic models used

Kinetic model	Slope	Intercept	R^2
Prout-Tompkins	2.041×10^{-3}	−1.956	0.8304
One-dimensional advance of phase boundary	-4.029×10^{-4}	0.8678	0.9411
Two-dimensional advance of phase boundary	2.776×10^{-4}	0.0531	0.9750
Three-dimensional advance of phase boundary	2.071×10^{-4}	0.0309	0.9833
One-dimensional diffusion	3.511×10^{-4}	−0.0293	0.9947
Two-dimensional diffusion	2.490×10^{-4}	−0.0349	0.9947
Three-dimensional diffusion	8.239×10^{-5}	−0.0163	0.9851
Power law, $n = 1/4$[a]	2.259×10^{-4}	0.6117	0.7691
Power law, $n = 1/3$[a]	2.720×10^{-4}	0.5208	0.7970
Power law, $n = 1/2$[a]	3.362×10^{-4}	0.3775	0.8457
Power law, $n = 1$[a]	4.029×10^{-4}	0.1322	0.9411

[a]It should be noted that while potentially descriptive, power laws hold no physical meaning.

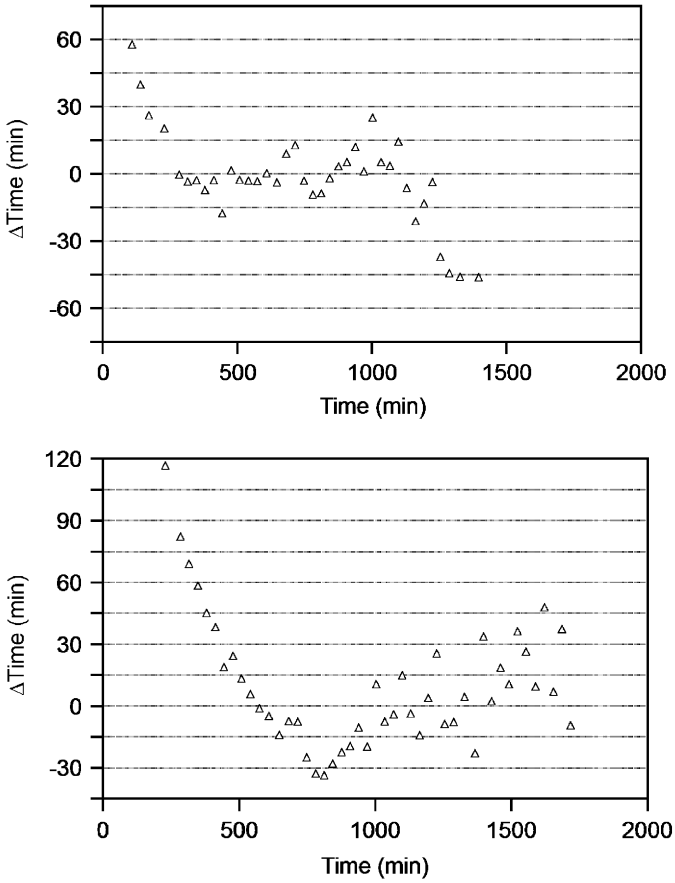

Fig. 6. Refined graph of time residuals (Δt vs. t) for one-dimensional diffusion (top), note the linear range from 285 to 1226 min. Unrefinable graph of time residuals (Δt vs. t) for three-dimensional diffusion (bottom), note that there does not appear to be any linear portion of the residual.

cannot be made to meet these criteria for at least some portion of the data, then the model is not likely to be an accurate description of this transition (see Fig. 6 (bottom)).

The Δt vs. t graphs of the two- and three-dimensional advance of phase boundary models were found to vary in a pseudo-parabolic fashion, and were, therefore, not considered to be suitable models to describe the transition. The three-dimensional diffusion model [28] was found to vary in a third-order fashion and, therefore, did not contain any significant linear portion, which could be further evaluated. The Δt vs. t residual plots of the one- and two-dimensional diffusion models were each found to contain a portion of data that varied linearly in time. The one- and two-dimensional diffusion models were each then applied exclusively using their respective linear ranges and further evaluated (see Table 2).

4. Discussion

To more completely convey the nature and relationship of the phases involved in the phase transition described, it is appropriate to first generally discuss the thermal behavior of Na_3PO_3S. DTA of α-Na_3PO_3S, performed under vacuum, reveals three thermal events in the temperature range of 25–650 °C [5]. A single endothermic event occurs upon heating at 561 °C, and two exothermic events occur upon cooling at 491 and 452 °C. All thermal events are reproducible on multiple cycles, and PXRD analysis of the residue after the DTA experiment shows it to be α-Na_3PO_3S [5]. (Slight differences in transition temperatures between this report and those in Ref. [5]. are due to differing heating/cooling rates used, leading to small differences in thermal lag.)

In situ neutron diffraction experiments at high temperature, using the Howe furnace, indicated that as α-Na_3PO_3S is heated, it converts to a new γ-phase at 561 °C [5,29]. The existence of this phase was unclear until now, as it was not able to be trapped upon quenching. Upon cooling, the γ-phase converts to the β-phase at 491 °C. The β-phase next converts back to the room-temperature stable α-phase upon cooling at 452 °C. The neutron powder diffraction patterns of each of these phases have been measured in situ at high temperatures and will be the topic of another forthcoming report [29].

While the β-phase is thermally stable between 452 and 491 °C, it has also been reported that this phase may be trapped by rapid cooling [5,6]. A DTA of the trapped

Table 2
Summary of linearization of potentially promising kinetic models

Kinetic model	Residual shape	Linear range (min)	Number of points $>\pm 15$ min[a]	R^2 of linear data range
Two-dimensional advance of phase boundary	Parabolic	N/A	N/A	N/A
Three-dimensional advance of phase boundary	Parabolic	N/A	N/A	N/A
One-dimensional diffusion	Partial linear	285–1226	3	0.9989
Two-dimensional diffusion	Partial linear	381–1523	6	0.9984
Three-dimensional diffusion	Third order	N/A	N/A	N/A

[a]This column denotes the number of data points within the linear range which do not fall within the 15 min tolerance window for calculated vs. observed values.

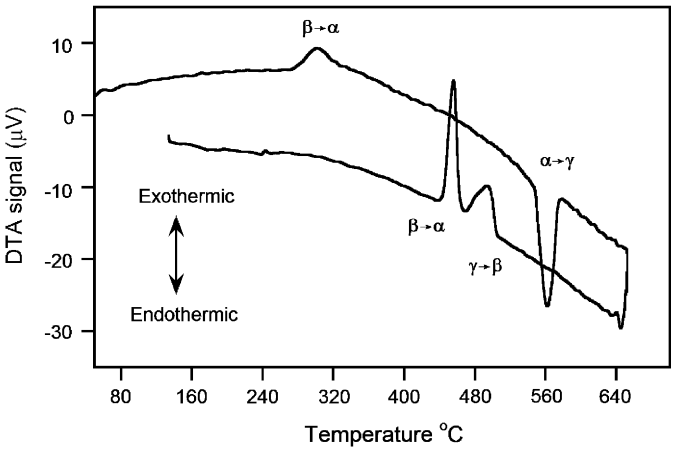

Fig. 7. DTA diagram of β-Na_3PO_3S obtained under vacuum. An irreversible exothermic event occurs on heating at ~300 °C and corresponds to the thermal relaxation of β-Na_3PO_3S to α-Na_3PO_3S. The remaining thermal events are reproducible on multiple cycles.

β-phase was also acquired (see Fig. 7). The DTA diagram of the sample of β-Na_3PO_3S is similar to that of the α-phase, except for an irreversible exothermic event upon heating at ~300 °C, followed by all of the same thermal events, which were observed for a sample of the α-phase. Similar to the thermal behavior of the α-phase, PXRD analysis of the DTA residue after thermal analysis shows the material to be α-Na_3PO_3S. This leads us to the conclusion that the quenched β-phase thermally converts to the α-phase at ~300 °C. The temperature at which the trapped β-phase thermally converts to the thermodynamically stable α-phase is important because it highlights the temperature suppression of 275 °C for this transition at room temperature due to RH.

The humid atmosphere used in the in situ neutron diffraction experiment was composed of D_2O due to the high coherent neutron scattering cross-section of deuterium, which would help to facilitate the observation of any hydrated phase, which might form during the course of the experiment. However, no such hydrated phase was observed. It is possible that the use of D_2O may give rise to an isotope effect in the determination of the kinetics of the reaction, but the existence or extent of this effect has not been determined.

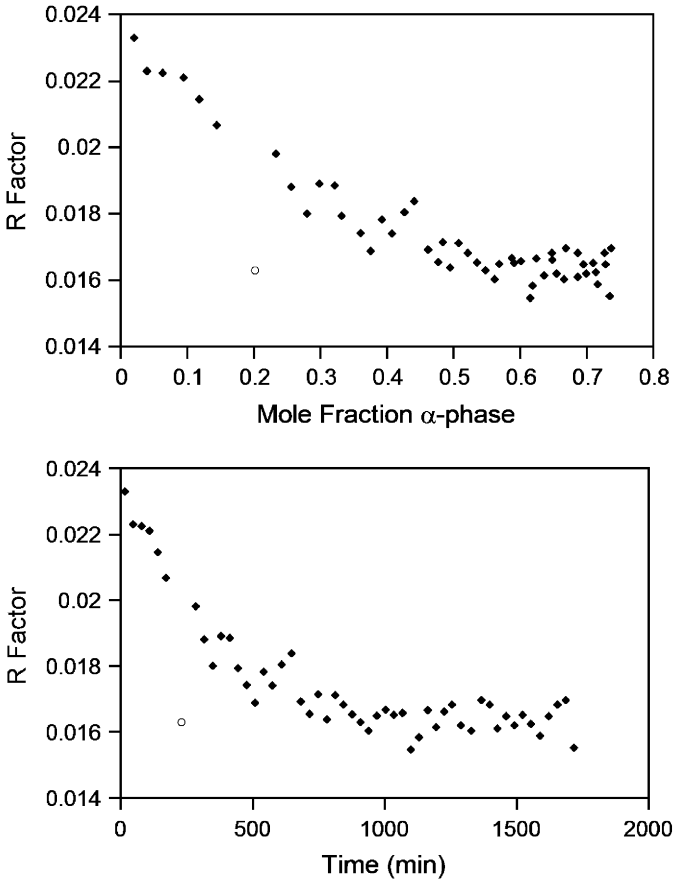

Fig. 8. Refined R factors as a function of the mole fraction of the α-phase (top). Refined R factors as a function of time (bottom).

The lack of an observable third phase during the course of the transition helps to validate the use of the two-phase linear combination model for the determination of sample composition. The use of this model can also be justified by the data that compose Fig. 8. All of the R factors determined throughout the course of the experiment are low ($<2.33\%$). The plot of R factor vs. time does seem to indicate some type of bias though, as the R factors at early times are systematically larger than those occurring later in the experiment. This effect is explained by the crystallinity of the predominant polymorph though time.

The quench process used to obtain β-Na_3PO_3S generates a phase having inherently poor crystallinity, resulting in a

low signal to noise ratio. α-Na_3PO_3S has an inherently higher degree of crystallinity (see Fig. 2). The linear combination method used to model the system is not able to differentiate noise from signal in either the transitioning sample or the reference pattern(s), making it more prone to poorer fits when the signal to noise ratio is lower. Thus, the portion of the transition that is predominantly the β-phase is more susceptible to poorer fits. This interpretation is justified by the point marked by an open circle in Fig. 8. The only difference between this data point and its surrounding neighbors is that the time of collection corresponding to this data point was ~50% longer than the others. The *R* factor corresponding to this increased collection, and consequently improved signal to noise ratio, is on par with those data points that occur later in the experiment, when the sample has predominantly converted to the α-phase.

The levels of the outgas humidity measured while the sample was in the gas flow (see Fig. 3) provide insight into the interaction of the solid with a humid gas. At early times during the experiment, the outgas humidity was consistently measured to be lower than the set value, indicating water missing from the outgas flow. Conversely, later in the experiment, the outgas humidity was measured to be greater than the set value, indicating a surplus of water in the outgas flow. This time-dependant behavior implies that the sample absorbs water out of a humid atmosphere, utilizes it to facilitate the phase transition, and extrudes it back into the atmosphere upon completion of the transformation. This type of behavior seems to support a diffusional model for the kinetics of the transition. The water must be absorbed from the gas flow, reducing the measured outgas humidity, diffuse though any already converted shell to the particle's unreacted core, where it catalyzes a phase transition and then either diffuses deeper to the still unreacted core, or diffuses back out of the particle into the gas stream, where it contributes to a higher-than-anticipated outgas humidity. Furthermore, the higher-than-anticipated outgas humidity measured during the release of water back into the gas flow supports the assertion that this transition, although catalyzed by water, yields an anhydrous product.

The two best fitting kinetic models, both of which are diffusion-based models, are plotted in their linearized forms in Fig. 9. Both models fail to accurately describe the data at either early or late experimental times. The slow kinetic rates early in the experiment are due to a lag time, a period of time during which crystallization occurs more slowly than expected while the system attempts to reach a steady state. One cause of this can be traced to the physical apparatus used during the neutron diffraction experiments. The humid gas flow had directionality relative to the sample and, as noted by the outgas humidity measurements, strongly interacts with the sample. It seems reasonable to infer that the humidity of the flow gas is not constant throughout the sample, but, at early times, is higher on the upstream side of the sample and lower on the

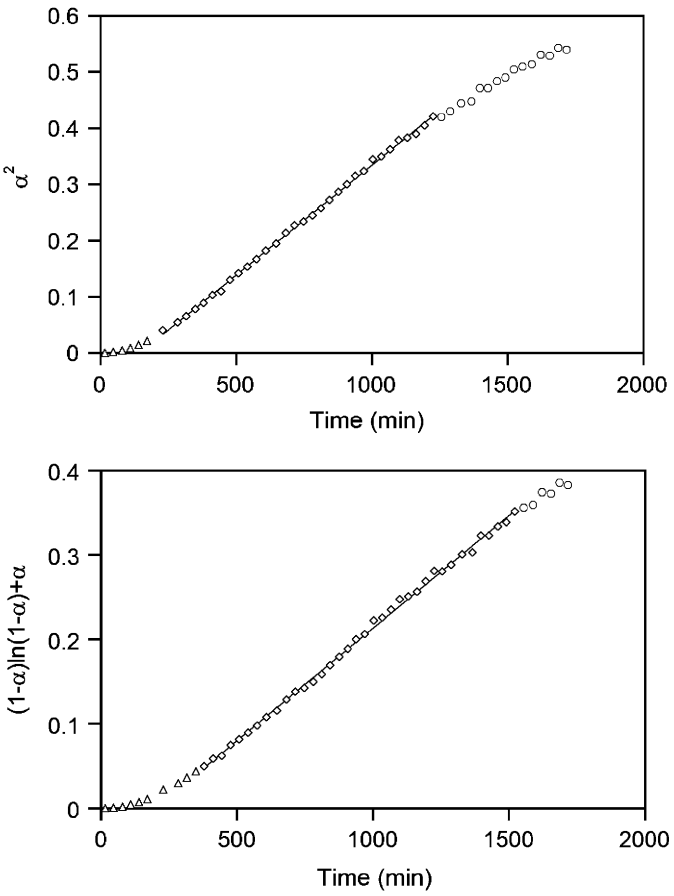

Fig. 9. Linearized form of the one-dimensional diffusion model plotted vs. time (top), and the linearized form of the two-dimensional diffusion model plotted vs. time (bottom). Triangles indicate lag time prior to equilibration of the flow gas humidity with the sample. Diamonds indicate the range over which the transition may be considered linear. Circles indicate slowing of the reaction at later times due to uncontrolled factors.

downstream side of the sample. This implies that the sample is not uniformly reacting to the humid gas flow, and some time is required to allow the sample to equilibrate with the humid gas flow before any kinetic rate equation can be meaningfully applied to the system. At later times in the experiment, the system begins to slow prematurely. This is a well-known failing of many solid-state kinetic models and originates from particle size dispersion and sample morphology [30].

The best fitting kinetic models support that the humidity-induced phase transition is a fundamentally diffusion driven process, which requires the reactant, water, to be transiently present in the interior of the particle for the transformation to take place. Unfortunately, the analysis of the data makes no clear distinction between the appropriateness of either the one- or two-dimensional diffusion models, and so a brief discussion of their assumptions, successes and failings is appropriate.

The one-dimensional diffusion model [28] may be applied to systems in which an isotropic material in a plate morphology is undergoing a diffusion-limited process

either with another solid, a liquid or a gas. This is due to the tremendous surface area available on the plate faces, relative to the area of the plate edges. There is another circumstance in which this model might hold true, and that is for an anisotropic material, undergoing a diffusion limited process in which one set of crystal faces have significantly lower diffusion energy barriers relative to those faces which are orthogonal to them. If the difference is indeed large enough, a diffusion limited process would appear to be one dimensional. The sample morphology would continue to have an effect on the kinetics of the transformation, but its importance would diminish greatly.

The two-dimensional diffusion model [28] may be applied to isotropic materials with an acicular morphology undergoing a diffusion-limited process with a solid, liquid or gas. The two-dimensional approximation of this model is again due to the tremendous area of the wire side relative to that of the top and bottom. Similar to the argument made above, this model may also be applied to anisotropic systems, if the barrier to diffusion is much greater in one direction than the other two. The sample morphology again will continue to play a role in the kinetics of the transformation, but with greatly diminished importance.

β-Na_3PO_3S has been previously indexed by Jansen et al. as hexagonal [6]. This assignment, if it is indeed correct, could support either possibility, as hexagonal materials have one dimension which is unique. If the unique direction were to have exceptionally low diffusion barriers relative to the other two, this would support the one-dimensional model; and if it were to have high-diffusion barriers relative to the other two, this would support the two-dimensional model. The present experiment is not able to differentiate between the two models, since matters that potentially affect the kinetic process such as particle size [31,32], size distribution, and morphology [7] were not considered prior to experimentation and, in some cases, are impossible to control, due to the sample preparation methods employed.

5. Conclusions

A phase transition from β-Na_3PO_3S to α-Na_3PO_3S, two anhydrous inorganic crystalline species, has been observed. The temperature of this transition has been determined to be suppressed by 275 °C by exposure to a humid atmosphere. Measurements of this humidity-induced phase transition have been made by in situ neutron powder diffraction. The sample phase composition through time was determined by an empirical whole pattern fitting method in the absence of structural knowledge of the β-phase. The kinetics of this transition has been determined to be either one- or two-dimensional diffusion. The diffusional character of the process is also supported by the observation that water was absorbed from the humid gas stream early in the experiment and later released from the sample back into the flowing gas stream. At no point during the course of the experiment was any hydrated phase observed to be present in the sample. Although no hydrated phase was observed, the requirements of the diffusional models, coupled with the absorption/desorption of the gaseous water, indicate that water must be intimately involved in the interior of the transitioning particles during this process. The exact nature of this involvement is not yet fully understood; but, we look forward to further experimentation to reveal more details of this phenomenon which is so unusual among solid-state inorganic materials [29].

Acknowledgments

The authors gratefully acknowledge the patient assistance of Mr. Evan Maxey and Dr. Jim Richardson of the Intense Pulsed Neutron Source at Argonne National Lab, especially for the careful design of the controlled-humidity apparatus. We also thank Argonne National Lab and the Intense Pulsed Neutron Source for beam time (IPNS-4557). Dr. Peter Wildfong also has our gratitude for extended discussions regarding the study of solid-state kinetics. NJT wishes to thank Duquesne University's Department of Chemistry and Biochemistry for the travel funds which made his trip to Argonne National Lab possible.

References

[1] A. Wurtz, Ann. Chim. Phys. 20 (1847) 472–482.
[2] C.J. Kubierschky, J. Prakt. Chem. 31 (1885) 93–111.
[3] E. Zintl, A. Bertram, Z. Anorg. Allg. Chem. 245 (1940) 16–19.
[4] M. Jansen, M. Pompetzki, Z. Anorg. Allg. Chem. 628 (2002) 641–646.
[5] N.J. Takas, J.A. Aitken, Inorg. Chem. 45 (2006) 2779–2781.
[6] M. Pompetzki, L. van Wüllen, M. Jansen, Z. Anorg. Allg. Chem. 630 (2004) 384–388.
[7] Y. Sugawara, A. Nakamura, Y. Iimura, K. Kobayashi, H. Urabe, J. Phys. Chem. B. 106 (2002) 10363–10368.
[8] S.R. Byrn, R.P. Pfeiffer, J.G. Stowell, Solid-State Chemistry of Drugs, SSCI Inc., Indiana, 1999, pp. 443–460.
[9] D. Burnett, F. Theilmann, J. Booth, Int. J. Pharm. 287 (2004) 123–133.
[10] E. Vadas, P. Toma, G. Zografi, Pharm. Res. 8 (1991) 148–155.
[11] L. Beneš, K. Meláádová, V. Zima, M. Trchová, E. Uhlířová, P. Matějka, Eur. J. Inorg. Chem. (2000) 895–900.
[12] M. Bartolomei, P. Bertocchi, E. Antoniella, A. Rodomonte, J. Pharmaceut. Biomed. 40 (2006) 1105–1113.
[13] J.B. Holt, I.B. Culter, M.E. Wadsworth, J. Am. Ceram. Soc. 45 (1962) 133–136.
[14] M.L. Foo, T. Klimczuk, R.J. Cava, Mater. Res. Bull. 40 (2005) 665–670.
[15] A.K. Sheridan, J. Anwar, Chem. Mater. 8 (1996) 1042–1051.
[16] A. Khawam, D.R. Flanagan, J. Pharm. Sci. 95 (2006) 472–498.
[17] T. Yoshinari, R.T. Forbes, P. York, Y. Kawashima, Int. J. Pharm. 247 (2002) 69–77.
[18] X. Xu, J.T. Han, D.H. Kim, K. Cho, J. Phys. Chem. B. 110 (2006) 2764–2770.
[19] C.J. Ellison, J.M. Torkelson, Nat. Mater. 2 (2003) 695–700.
[20] Y. Masuda, K. Hashimoto, Y. Ito, Thermochim. Acta 163 (1990) 271–278.
[21] S.K. Yasuda, J.L. Lambert, Inorg. Syn. 5 (1957) 102–104.
[22] 〈http://www.pns.anl.gov/ngs/ancillary/Sample%20Environments/Howe_Furnace.html〉 (2007).

[23] T. Worlton, ISAW: Integrated Spectral Analysis Workbench, v. 1.8.0, 2006. 〈http://www.pns.anl.gov/ISAW/〉. Intense Pulsed Neutron Source.
[24] E. Maxey, J. Richardson, unpublished work.
[25] T. Egami, S.J.L. Billinge, Underneath the Bragg Peaks: Structural Analysis of Complex Materials, Pergamon Press, New York, 2003, pp. 26,37.
[26] Microsoft® Office Excel 2003, Copyright 1985–2003, Microsoft Corporation.
[27] L.S. Ladson, A.D. Waren, A. Jain, M. Ratner, ACM T. Math. Software 4 (1978) 34–50.
[28] J.H. Sharp, G.W. Brindley, B.N.N. Achar, J. Am. Ceram. Soc. 49 (1966) 379–382.
[29] N.J. Takas, J.A. Aitken, work in progress.
[30] R.E. Carter, J. Chem. Phys. 34 (1961) 2010–2015.
[31] P.T. Cardew, R.J. Davey, A.J. Ruddick, I. Chem. E. Symposium Series No. 69. pp. 123–133.
[32] F. Huang, J.F. Banfield, J. Am. Chem. Soc. 127 (2005) 4523–4529.